



HAL
open science

Dewetting of a thin polymer film under shear

Kheireddine Kadri, Jorge Peixinho, Thomas Salez, Guillaume Miquelard-Garnier, Cyrille Sollogoub

► **To cite this version:**

Kheireddine Kadri, Jorge Peixinho, Thomas Salez, Guillaume Miquelard-Garnier, Cyrille Sollogoub.
Dewetting of a thin polymer film under shear. *Polymer*, 2021, 235, pp.124283. hal-03430865v1

HAL Id: hal-03430865

<https://hal.science/hal-03430865v1>

Submitted on 20 Jul 2021 (v1), last revised 16 Nov 2021 (v2)

HAL is a multi-disciplinary open access archive for the deposit and dissemination of scientific research documents, whether they are published or not. The documents may come from teaching and research institutions in France or abroad, or from public or private research centers.

L'archive ouverte pluridisciplinaire **HAL**, est destinée au dépôt et à la diffusion de documents scientifiques de niveau recherche, publiés ou non, émanant des établissements d'enseignement et de recherche français ou étrangers, des laboratoires publics ou privés.

Dewetting of a thin polymer film under shear

K. Kadri^a, J. Peixinho^a, T. Salez^b, G. Miquelard-Garnier^a, C. Sollogoub^a

^aLaboratoire PIMM, Arts et Métiers, CNRS, Cnam, Hesam Université, 151 boulevard de l'Hôpital, Paris, France

^bUniv. Bordeaux, CNRS, LOMA, UMR 5798, F-33405 Talence, France

Abstract

The objective of this work is to study the role of shear on the rupture of ultra-thin polymer films. To do so, a finite-difference numerical scheme for the resolution of the thin film equation was set up taking into account capillary and van der Waals (vdW) forces. This method was validated by comparing the dynamics obtained from an initial harmonic perturbation to established theoretical predictions. With the addition of shear, three regimes have then been evidenced as a function of the shear rate. In the case of low shear rates the rupture is delayed when compared to the no-shear problem, while at higher shear rates it is even suppressed: the perturbed interface goes back to its unperturbed state over time. In between these two limiting regimes, a transient one in which shear and vdW forces balance each other, leading to a non-monotonic temporal evolution of the perturbed interface, has been identified. While a linear analysis is sufficient to describe the rupture time in the absence of shear, the nonlinearities appear to be essential otherwise.

Keywords: Thin films, Lubrication, Polymers, Dewetting, Shear, Nanolayer coextrusion

1. Introduction

2 Nanolayer coextrusion, an innovative process allowing the combination
3 of at least two polymers in a stratified film or membrane having a total
4 thickness on the order of 100 μm but composed of thousands of alternating
5 nanometric layers, has gained an increased interest in the past few years [1, 2].
6 This process offers unique opportunities to explore fundamental questions on
7 the effects of confinement on polymer properties, such as crystallization [3],
8 chain mobility and structural relaxation [4, 5, 6] or interfacial phenomena

9 [7, 8, 9], as well as to design new nanostructured materials with novel or
10 enhanced properties (mechanical, optical, conductive, gas barrier properties,
11 etc.) [10].

12 However, one strong limitation of the process lies in possible layer breakups,
13 observed by several authors on different polymer pairs when reducing the
14 layer thickness [11, 12, 13]. In a previous study, we investigated this phe-
15 nomenon in polystyrene (PS)/poly(methyl methacrylate) (PMMA) nanolay-
16 ered films [14] and evidenced the existence of a critical thickness around 10
17 nm, below which the layers rupture spontaneously, independently of the pro-
18 cessing conditions. We then proposed a mechanism responsible for this layer
19 breakup, similar to the one leading to the dewetting of an ultra-thin polymer
20 monolayer deposited on a solid substrate, as firstly observed by Reiter et al.
21 [15] and subsequently explained by Brochard et al. [16].

22 In nanolayer coextrusion, when the layer thickness is very small - typically
23 below 100 nm-, attractive long-range forces (*i.e.* van der Waals forces) be-
24 tween the two adjacent layers cannot be neglected. Below a critical thickness
25 around 10 nm, they become dominant over the stabilizing capillary forces.
26 In consequence, they may amplify any interfacial instability such as the one
27 due to thermal fluctuations, eventually leading to the layer breakup. Sev-
28 eral model experiments on spin-coated three-layer systems were subsequently
29 proposed to confirm this scenario [17, 18]. Comparing the characteristic
30 dewetting times in a model trilayer system to typical residence times in the
31 nanolayer coextrusion process, we also suggested that the shear induced in
32 the nanolayer process may delay the layer rupture, *i.e.* may stabilize the
33 layers against rupture.

34 Similar questions have been addressed for many years in the field of fluid
35 mechanics, where the stability of ultra-thin liquid films has been a concern in
36 several industrial applications, such as coating processes [19] or lithographic
37 printing [20]. The stability of thin films has been the subject of many theo-
38 retical and experimental studies (see for example the reviews of Oron et
39 al. [21] and Craster et al. [22]). The pioneering works of Vrij [23] and
40 Sheludko [24] focused on the mechanism of spontaneous rupture of a thin
41 liquid film deposited on a solid substrate. Using slightly different approaches
42 - thermodynamic treatment for Sheludko and diffusion equation for Vrij-,
43 they showed for the first time that the amplification by vdW forces of small
44 irregularities at the film's free surface may lead to a decrease of the total free
45 energy despite the increasing surface, and consequently induce film rupture.
46 They proposed a critical thickness below which the destabilizing vdW forces

47 become dominant over the capillary forces, a critical wavelength of the initial
48 irregularities above which the film is unstable, as well as a growth rate of the
49 perturbation and a characteristic time for rupture.

50 A more systematic and rigorous approach, developed by Ruckenstein and
51 Jain [25], was based on a linear stability analysis of the Navier-Stokes equa-
52 tions. They assumed that the amplification of small perturbations at the
53 film interface generates a flow in the film. Due to its small thickness, the
54 lubrication approximation was employed. The long-range vdW forces were
55 accounted for through a disjoining pressure term as proposed by Derjaguin
56 [26]. Even if this stability analysis is theoretically valid for small perturba-
57 tions only, information about the conditions leading to film rupture could
58 be obtained. In particular, Ruckenstein and Jain showed that the critical
59 wavelength of the initial periodic disturbance leading to rupture was much
60 larger than the film thickness. These results laid the groundwork for sub-
61 sequent studies that investigated the nonlinear effects on thin film rupture
62 using either a perturbative analysis [27] or numerical computations [28]. In
63 the latter study, the authors derived a highly non-linear partial differential
64 equation, a so-called thin film equation, that describes the evolution of the
65 surface of a thin film subject to: i) viscous stresses, ii) a stabilizing Laplace
66 pressure, and iii) a destabilizing disjoining pressure. The main qualitative
67 features of the rupture in these nonlinear studies were similar to the ones in
68 the linear analysis. Still, some quantitative differences were obtained con-
69 cerning the breakup time in particular, that was found to be systematically
70 inferior in the nonlinear studies compared to the linear analysis. This is likely
71 due to the fact that the latter analysis underestimates the destabilizing effect
72 of the long-range forces. Those various approaches were extended later to
73 multilayer films [20, 29, 30].

74 The effect of a shear flow on a thin film rupture was first explored by
75 Kalpathy et al. [31] for a liquid-liquid interface in a stratified flow and by
76 Davis et al. [32] in a thin liquid film. They showed that when shear is
77 imposed, the film rupture is delayed and that above a critical shear rate,
78 the rupture is even suppressed. Beyond purely hydrodynamic explanations,
79 another possible effect in practical systems could be the shear-induced mod-
80 ification of the seed thermal fluctuations [33, 34].

81 In the present study, we investigate the impact of shear on the stability of
82 a polymer thin film, using a numerical approach [35] inspired by Bertozzi
83 and Zhornitskaya [36, 37]. In particular, by systematically studying various
84 combinations of shear rates and Hamaker constants governing the intensity

85 of vdW forces, we discuss the existence of several regimes for the thin film
 86 stability.

87 2. Problem position and model

88 2.1. Problem position

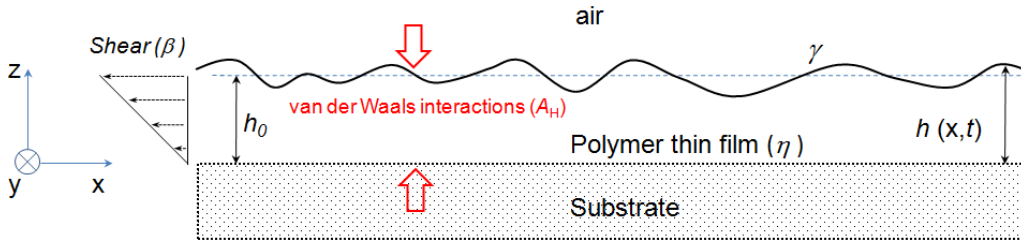


Figure 1: A viscous polymer film, of viscosity η and nominal thickness h_0 , is placed atop a rigid substrate. External shear rate β , surface tension γ and van der Waals forces (with Hamaker constant A_H) compete with each other, and generate a viscous flow that can either result in growth or damping of an initial interfacial perturbation. At horizontal position x and time t the film profile is $h(x,t)$. Invariance along y is assumed.

89 The problem studied is represented in Figure 1. A glassy polymer (such
 90 as PS) thin film of nominal thickness h_0 typically below 100 nm is lying on
 91 a substrate and heated well above its glass transition temperature T_g . For a
 92 PS film, T_g is about 100°C and the temperature of the study, similar to the
 93 processing temperature, would be close to 200°C. At this temperature, the
 94 polymer can be considered as a Newtonian fluid with a constant viscosity
 95 η_0 , on the order of 10^4 Pa.s. The viscosity depends on molecular weight,
 96 but the value indicated here is typical of polymers used in extrusion [14].
 97 The surface tension of the polymer with air is noted γ (~ 27.7 mN/m for
 98 PS at 200°C [38]) and the Hamaker constant for the substrate/polymer/air
 99 system is noted A_H . The value of the latter is difficult to measure experi-
 100 mentally, and though the typical order of magnitude of Hamaker constants
 101 is similar for most systems, i.e. $\sim 10^{-19}$ J, several values can be found
 102 in the literature. For an air/PS/SiO₂ system, Seemann et al. [39] provide
 103 $A_{H_{\text{air/PS/SiO}_2}} = 2.2 \cdot 10^{-20}$ J, similar to the value obtained using material re-
 104 fractive indices and dielectric constants from the literature [40, 41]. In the
 105 present study, to limit the numerical rupture time which increases with de-
 106 creasing values of the Hamaker constant, we employ A_H to values between 5

107 10^{-19} and $5 \cdot 10^{-18}$ J. Shear, characterized by a shear rate β , is applied from
 108 right to left. Different values of shear rates will be explored, and their effect
 109 on an interfacial perturbation monitored through the evolution of the profile
 110 thickness $h(x, t)$ over time t and space along the x -axis.

111 2.2. Governing equation

112 Taking into account the previous considerations and a spatial invariance
 113 along the horizontal direction y , the general thin film equation [21] is assumed
 114 to describe the dynamics of the thickness profile $h(x, t) = h_0 + \delta h(x, t)$, where
 115 $\delta h(x, t)$ is the perturbation field with respect to h_0 . The thin viscous film
 116 is experiencing Laplace and disjoining pressures, as well as shear stresses.
 117 Neglecting gravitational forces, the thin film equation reads in our case:

$$\partial_t h + \frac{\gamma}{3\eta} \partial_x \left(h^3 \partial_x^3 h + \frac{3A_H}{6\pi\gamma h} \partial_x h \right) - \beta h \partial_x h = 0 . \quad (1)$$

118 Interfacial tension and viscosity are considered constant and possible
 119 changes as a function of the film thickness are also neglected in this study.
 120 To solve numerically the equation, one introduces the following dimensionless
 121 variables and parameters:

$$\begin{aligned} H = \frac{h}{h_0} \quad ; \quad \Delta H = \frac{\delta h}{h_0} \quad X = \frac{x}{h_0} \quad ; \quad T = \frac{\gamma t}{3\eta h_0} \quad ; \quad \Lambda = \frac{\lambda}{h_0} \\ K = kh_0 = \frac{2\pi}{\Lambda} \quad ; \quad A = \frac{A_H}{6\pi\gamma h_0^2} \quad ; \quad B = \frac{3\eta\beta h_0}{2\gamma} , \end{aligned} \quad (2)$$

122 where λ is the wavelength of the initial harmonic perturbation (see below)
 123 and k is the associated angular wavenumber. Note that both A and B depend
 124 on the nominal film thickness and surface tension. The dimensionless thin
 125 film equation can then be written as:

$$\partial_T H + \partial_X \left[H^3 \left(\partial_X^3 H + 3AH^{-1} \partial_X H \right) \right] - 2BH \partial_X H = 0 . \quad (3)$$

126 The parameters of the study and the ranges over which they have been
 127 varied are summarized in Table 1.

128

| Parameters | | | Dimensionless parameters | |
|------------|---|-----------|--------------------------|-----------------|
| h_0 | A_H | β | A | B |
| nm | J | s^{-1} | | |
| [10–100] | $[5 \times 10^{-19} - 5 \times 10^{-18}]$ | [0.2–200] | [0.001–0.1] | $[10^{-5} - 1]$ |

Table 1: Explored ranges for the parameters of the problem.

129 *2.3. Numerical method and boundary conditions*

130 The numerical procedure used here is a finite-difference method for thin-
131 film flows [35]. Specifically, we aim at following the temporal and spatial
132 evolution of an initial harmonic perturbation of wavelength λ . In contrast
133 to previous studies (Davis et al. [32] or Kalpathy et al. [31]), we do not
134 use periodic lateral boundary conditions here, but a large spatial window
135 size instead. To optimize the computational time and to limit the artificial
136 lateral boundary effects, we consider a truncated initial perturbation, with
137 1.5 periods, completed at its edges by a flat profile. We impose flat conditions
138 at the boundaries of the numerical domain. Finally, we have checked that
139 the chosen number of periods at the center and the size of the spatial window
140 do not affect the results.

141 At $T = 0$, the initial profile of the film is spatially discretized over M
142 segments, with a fixed spatial step ΔX and a spatial index $i \in [0, M - 1]$, as:

$$H[\Delta X(i - i_0), 0] = 1 + \Delta H \cos[2\pi\Delta X(i - i_0)/\Lambda] , \quad (4)$$

143 where i_0 is the index of the window center.

144 The numerical integration of Equation (3) along time T is then performed
145 using a 4th-order Runge-Kutta scheme [35]. In order to be self-consistent
146 with the lubrication framework and with the window-size constraint above,
147 we impose the following scale separation: $\Delta X \ll \Lambda \ll M\Delta X$.

148 **3. Results**

149 *3.1. Linear stability analysis*

The effect of shear on the stability of a thin film can be estimated, as
a first attempt, using a linear stability analysis. We stress that while such
an approach allows one in principle to predict whether an infinitesimal dis-
turbance at the surface is amplified or attenuated, it does not allow for the

quantitative study of rupture, which is outside the scope of linearity. We consider the evolution of an initial harmonic perturbation of small amplitude ΔH_0 around the nominal dimensionless thickness of the film (equals to 1). The perturbative field ΔH comprises a time-dependent factor $e^{\Gamma T}$, where Γ is the growth rate of the perturbation (the perturbation is amplified if $\Gamma > 0$ and damped if $\Gamma < 0$) and a space-dependent oscillatory factor e^{iKX} :

$$H = 1 + \Delta H \tag{5a}$$

$$\Delta H = \Delta H_0 e^{\Gamma T} e^{iKX} . \tag{5b}$$

150 This leads, after substitution in Equation (3), to the following dispersion
151 relation:

$$\Gamma = K^2(3A - K^2) + 2BiK . \tag{6}$$

152 The growth rate of the perturbation is a complex number, with a real
153 part Γ_R and an imaginary part Γ_I . The real part evaluates the actual rate at
154 which the perturbation is amplified or damped. It appears to be independent
155 of the shear and thus coincides with the solution of the no-shear case, *i.e.*
156 for $B = 0$ (see [25, 28]). A consequence of such a feature is that a numerical
157 treatment of the non-linear (*i.e.* beyond linear analysis) thin film equation
158 will be needed in order to understand further the potential role of shear
159 in the dewetting process. The evolution of Γ_R as a function of K , obtained
160 from Equation (6), is shown in Figure 2 and compared to numerical solutions
161 of Equation (3), for different values of A , including ones outside the range
162 studied later on with shear. It can be seen that in all cases the numerical
163 results are self-consistently in quantitative agreement with the analytical
164 prediction. Besides, one observes a maximum $\Gamma_{\max} = \Gamma(K_{\max})$, defined by:

$$K_{\max} = \sqrt{\frac{3A}{2}} \tag{7}$$

$$\Gamma_{\max} = \frac{9}{4} A^2 .$$

165 Note that the wavelength $\Lambda_{\max} = 2\pi/K_{\max}$ of this fastest growing mode will
166 be used as a wavelength Λ in all numerical computations below, in order to
167 reduce the total computational time.

168 Due to the imaginary part Γ_I , the perturbation is transported and shifted
169 in the shear direction. This shift is explicitly highlighted when injecting
170 Equation (6) into Equation (5), leading to:

$$\Delta H = \Delta H_0 e^{\Gamma_R T} e^{iK(X+2BT)} . \tag{8}$$

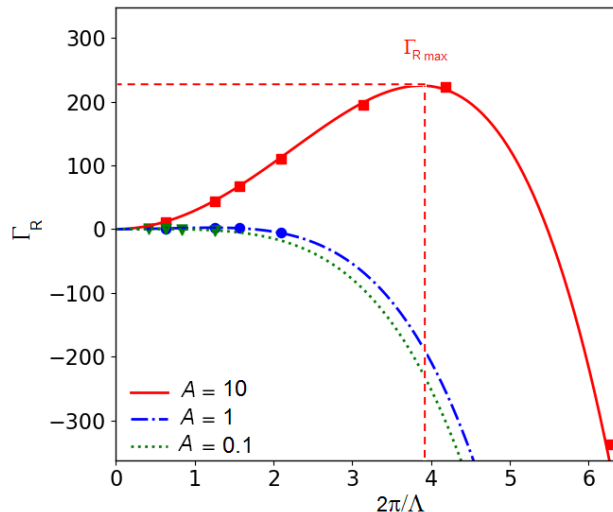


Figure 2: Real part Γ_R of the growth rate of the perturbation as a function of the angular wavenumber $K = 2\pi/\Lambda$, as obtained from Equation (6) (lines), as well as from numerical solutions of Equation (3) (symbols), for different values of the dimensionless Hamaker constant A , as indicated.

171 Thus, the perturbation propagates along $-X$ (i.e. the shear direction) with
 172 a speed equal to $2B$.

173 3.2. Rupture without shear

174 Here, an initial harmonic perturbation with an amplitude $\Delta H_0 = 0.1$ is
 175 considered, and Equation (3) is solved with $B = 0$. Due to vdW forces,
 176 the film may undergo a possible rupture after a time which depends on the
 177 value of the dimensionless Hamaker constant A . Since the numerical scheme
 178 is only stable for strictly positive H values, a criterion for rupture has been
 179 set as the time T_R at which the spatial minimum of H reaches 0.1. We have
 180 checked that other small-enough values of this arbitrary threshold do not
 181 change qualitatively the results.

182 A typical evolution of the film profile is given in Figure 3 for $A =$
 183 0.01. It is seen that the amplitude of the interfacial perturbation increases
 184 monotonously over time, until the film ruptures (at $T_R = 4800$ in this case,
 185 with our criterion above).

186 We now turn to the detailed study of the rupture time. First, the ef-
 187 fect of the initial amplitude of the perturbation is presented in Figure 4a for

188 different values of A . Apart from a numerical prefactor of order unity, the de-
 189 crease of the dimensionless rupture time T_R with increasing initial amplitude
 190 ΔH_0 as measured from our numerical solutions follows the linear-stability
 191 extrapolation law proposed by Sharma [27]:

$$T_R = \frac{1}{\Gamma_{\max}} \ln \left(\frac{1}{\Delta H_0} \right) . \quad (9)$$

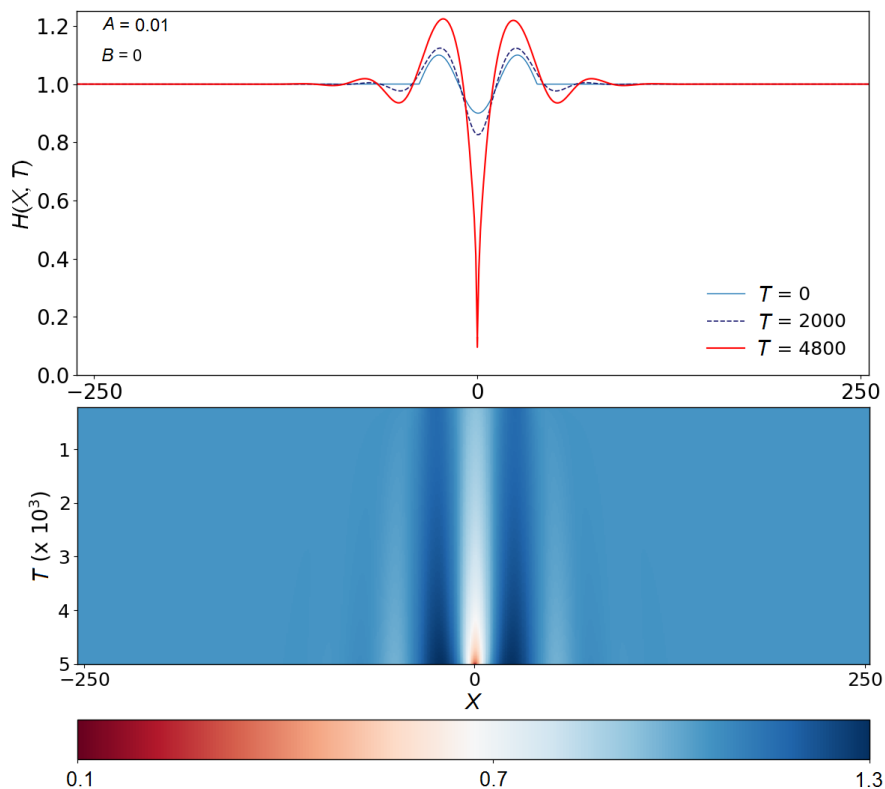


Figure 3: (top) Film profiles $H(X, T)$ versus the horizontal position X , at three different times T as indicated, as obtained from the numerical solution of Equation (3) with $A = 0.01$ and $B = 0$, for an initial harmonic perturbation with $\Delta H_0 = 0.1$ and $\Lambda = \Lambda_{\max}$. (bottom) Spatiotemporal diagram of the interfacial evolution, with X and T as axes, and the magnitude of H represented using the color code indicated below.

192 We stress that the expression predicted by Sharma is equivalent to the
 193 one by Ruckenstein [25] provided that $\Delta H_0 = 1/e$. Indeed, the expression of
 194 Ruckenstein corresponds by definition to the time constant of the exponen-
 195 tial growth and is therefore independent of ΔH_0 . Similarly, Ruckenstein's

196 expression is similar to the one predicted by Vrij [23], the two expressions
 197 quantitatively differing by a factor 2 only. These three theoretical estimates
 198 of T_R come from a similar linear approximation, and differ only by the exact
 199 convention chosen.

200 Putting back dimensions, Equation (9) is equivalent to:

$$t_R = \frac{48\pi^2\gamma\eta h_0^5}{A_H^2} \ln\left(\frac{h_0}{\delta h_0}\right), \quad (10)$$

201 where δh_0 is the initial amplitude of the perturbation.

202 As a guide for practical purposes, and using the values of the physical param-
 203 eters η and γ provided above, the rupture time t_R is plotted in Figure 4b as
 204 a function of the ratio h_0^5/A_H^2 , with real units, for the case where $\delta h_0/h_0=0.1$.

205 Apart from the numerical prefactor of order unity already mentioned
 206 above, it appears that Sharma's prediction describes well the data over 10
 207 decades. This suggests that non-linear effects are not essential to understand
 208 the main qualitative features of the film rupture process – under no shear.

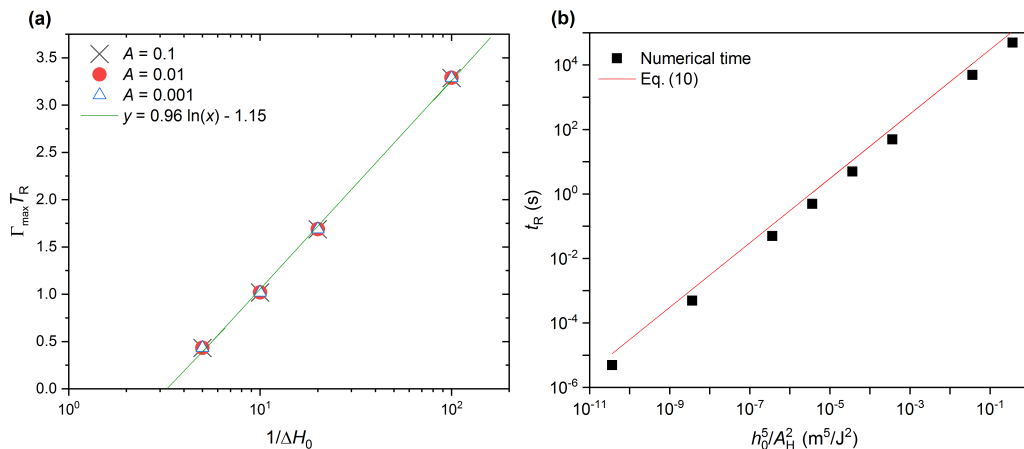


Figure 4: (a) Dimensionless rupture time T_R as a function of the inverse of the dimensionless perturbation amplitude ΔH_0 , for different values of the dimensionless Hamaker constant A . The solid line is a best fit to Eq. (9). (b) Dimensioned version of the rupture times obtained for $\delta h_0/h_0=0.1$ in panel a) with the values of interest presented in Table 1. The solid line is Eq. (10).

209 *3.3. Effects of shear*

210 *3.3.1. Influence of the shear rate*

211 Various finite shear rates ($B \neq 0$) have been tested within the same nu-
 212 merical framework as the one described above. The low-shear-rate behavior
 213 ($B \ll A$) is presented in Figure 5a, while the high-shear-rate behavior (B
 214 $\gg A$) is presented in Figure 5b. Over time, the perturbation moves along
 215 the x -axis in the direction in which the shear is applied, from right to left.
 216 At low shear rates, the behavior is similar to what is observed without shear:
 217 the perturbation grows with time and eventually leads to film rupture. At
 218 high shear rates, however, the perturbation is damped, leading to what could
 219 be described as a healing of the interface (*i.e.* going back to an unperturbed
 220 flat initial state) at long times.

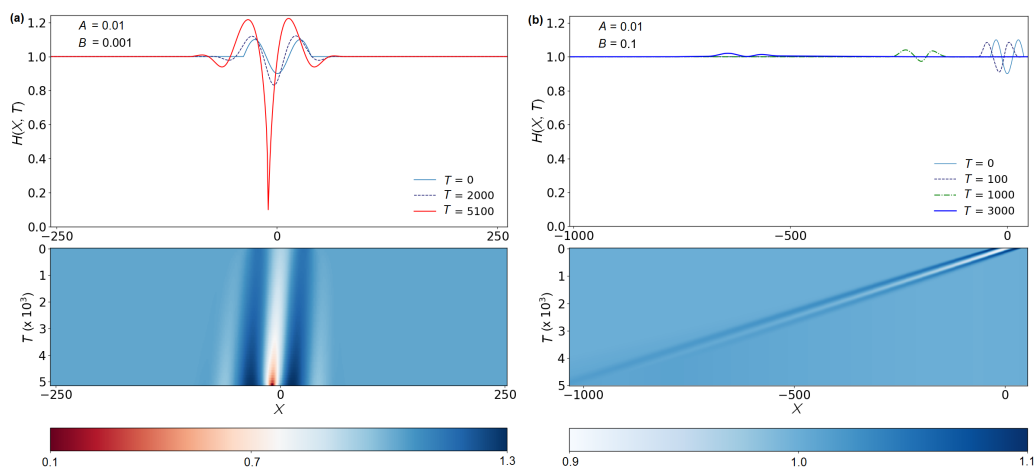


Figure 5: (top) Film profiles $H(X, T)$ versus the horizontal position X , at three different times T as indicated, as obtained from the numerical solutions of Equation (3) with $A = 0.01$, for an initial harmonic perturbation with $\Delta H_0 = 0.1$ and $\Lambda = \Lambda_{\max}$. The dimensionless shear rates are fixed to $B = 0.001$ and $B = 0.1$, in panels (a) and (b) respectively. (bottom) Corresponding spatiotemporal diagrams of the interfacial evolutions, with X and T as axes, and the magnitude of H represented using the color codes indicated below.

221 *3.3.2. Critical shear rate*

222 To understand more quantitatively the effect of shear on the perturbed
 223 interface profile, the maximum H_{\max} and minimum H_{\min} of the latter are
 224 plotted in Figure 6 as functions of time, and for different shear rates. At low

225 shear rate, it is seen that the time of rupture increases compared to the case
 226 without shear. At high shear rate, healing is confirmed by the fact that both
 227 extrema converge to 1, *i.e.* towards the flat-interface situation.

228

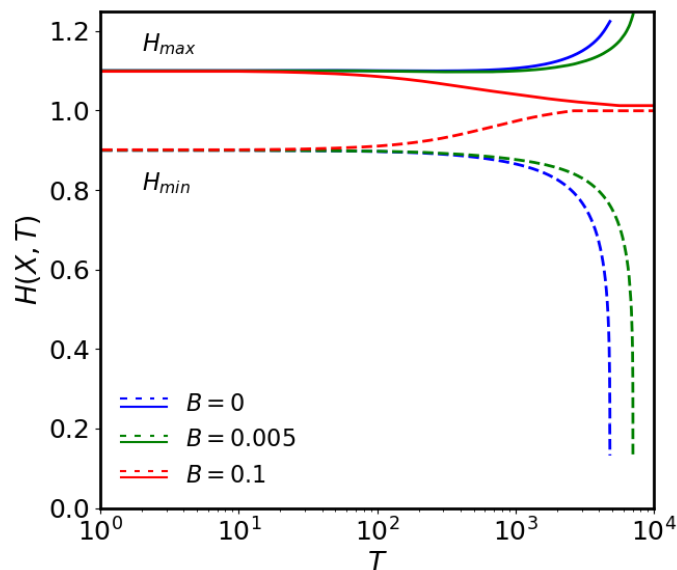


Figure 6: Temporal evolution of the maximum (H_{\max}) and minimum (H_{\min}) values of the dimensionless film profile, for three applied dimensionless shear rates, $B = 0, 0.005, 0.1$, as obtained from numerical evolutions such as the ones in Figure 5.

229 It is now interesting to examine what happens at intermediate shear rates,
 230 *i.e.* B close to A . Typical results are presented in Figure 7. Here, over the
 231 total computational time, no rupture is observed, but no healing either. As
 232 seen in the inset, the evolution of the perturbation, characterized as in Figure
 233 6, is not monotonic, suggesting the existence of a transient regime where vdW
 234 forces and shear compete with each other over times longer than the total
 235 time computed.

236 We now investigate the influence of shear on the film rupture. Figure 8
 237 shows the dimensionless rupture time T_R as a function of the dimensionless
 238 shear rate B . For low shear rates, the rupture time is only slightly higher
 239 than the value without shear. Then, for values of B higher than ~ 0.005 , T_R
 240 increases sharply, and becomes higher than the total computational time for
 241 $B > 0.014$. For $B > 0.03$, perturbation damping and healing of the interface
 242 are observed. A so-called "transient regime" is observed for $0.014 < B <$

243 0.03. A similar trend was found in a previous numerical simulation (Davis
 244 *et al.* [32]) using periodic boundary conditions with a coarse calculation
 245 domain. Specifically, Davis *et al.* [32] observed that the rupture is suppressed
 246 for $B \approx 10A$. The current systematic study allows us to construct a novel
 247 phase diagram, exhibiting in particular: i) perturbation damping for values
 248 as low as $B = 3A$; ii) the existence of a narrow transient regime with a non-
 249 monotonic variation of the interface profile along time, resulting in neither
 250 rupture nor healing within the accessed temporal and spatial window.

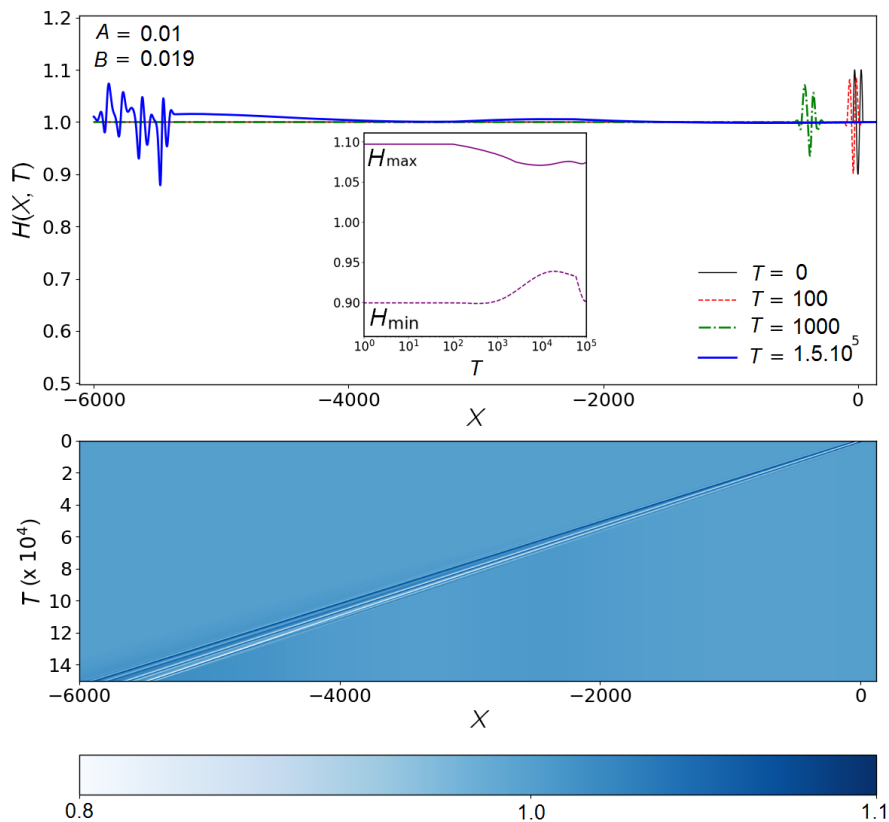


Figure 7: (top) Film profiles $H(X, T)$ versus the horizontal position X , at four different times T as indicated, as obtained from the numerical solution of Equation (3) with $A = 0.01$ and $B = 0.019$, for an initial harmonic perturbation with $\Delta H_0 = 0.1$ and $\Lambda = \Lambda_{\max}$. Inset: temporal evolutions of the profile's extrema, as in Figure 6. (bottom) Corresponding spatiotemporal diagram of the interfacial evolution, with X and T as axes, and the magnitude of H represented using the color code indicated below.

251

252 Interestingly, a natural dimensionless critical shear rate B_c can be identi-
 253 fied in the model. Indeed, by balancing the Hamaker and shear contributions
 254 in Equation (3), recalling that we have set $K = K_{\max}$, and invoking Equa-
 255 tion (7), one gets:

$$B_c \sim 3AK \sim 3\sqrt{\frac{3}{2}}A^{3/2}. \quad (11)$$

256 For $A = 0.01$, the latter estimate gives $B_c \approx 0.0037$, which corresponds
 257 approximately to the onset value of B in Figure 8 after which T_R sharply
 258 increases with B .

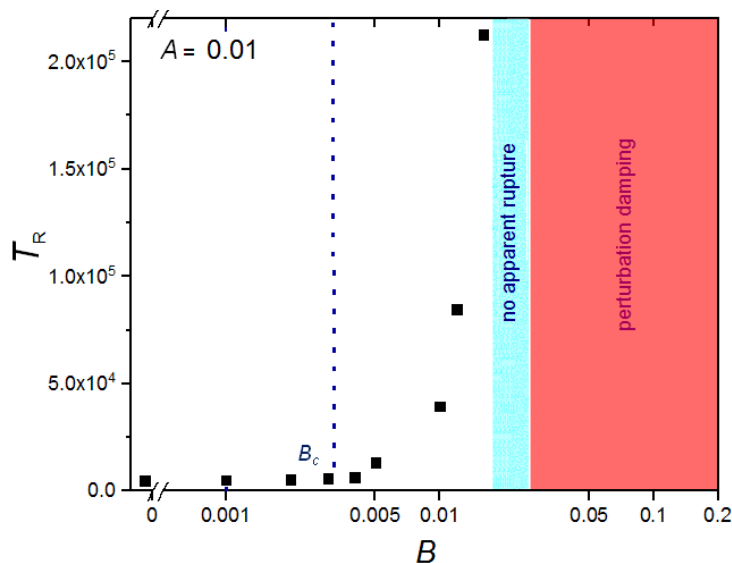


Figure 8: Dimensionless rupture time T_R as a function of the dimensionless applied shear rate B , for a dimensionless Hamaker constant $A = 0.01$. When T_R becomes larger than the total computational time, no rupture is observed, and for large enough B healing of the profile is even observed, as summarized by the colored areas. The vertical dashed line indicates $B_c \approx 3.7 \cdot 10^{-3}$, according to Equation (11).

259 The study above can be reproduced for several values of A . A similar
 260 trend is systematically recovered (not shown). Furthermore, a master curve
 261 is obtained in Figure 9, when plotting the ratio of the rupture time with shear
 262 and the rupture time without shear as a function of the ratio B/A . First, we
 263 recover the monotonic increase of the rupture time with shear rate. Secondly,
 264 the master rescaling is expected if, near a rupture event, one neglects the

265 capillary Laplace contribution over the Hamaker one in Equation (3), divide
 266 the whole equation by A , and absorb A in the definition of time.

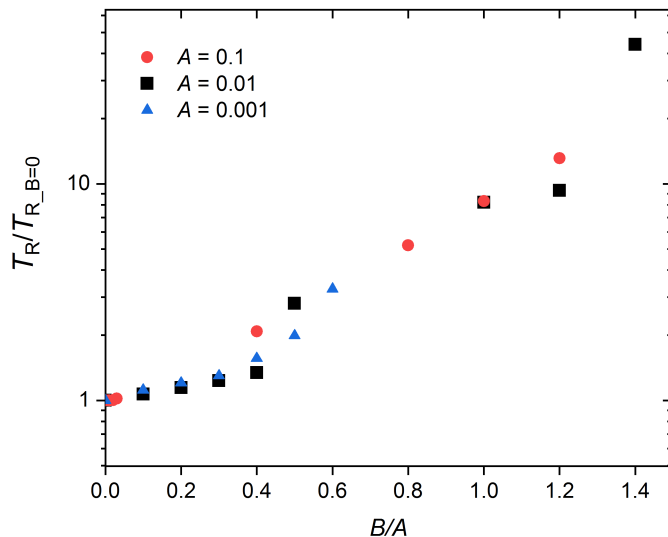


Figure 9: Rupture time rescaled with the no-shear rupture time as a function of the ratio between dimensionless shear rate B and dimensionless Hamaker constant A , for different values of A , as indicated.

267 Finally, let us discuss the layer stability in nanolayer coextrusion, from
 268 the results obtained here. In our study [14] on a PS/PMMA multilayer
 269 system, we made the hypothesis that rupture in multilayer films is induced
 270 by thermal fluctuations of amplitude $\sqrt{k_B T / \gamma} \sim 10^{-9}$ m (where k_B is the
 271 Boltzmann constant) [42] at the interface between adjacent layers, that are
 272 then amplified by vdW forces. Balancing capillary forces with vdW ones, the
 273 critical thickness was defined as:

$$h^* \sim \left(\frac{A_H}{3\pi\gamma} \right)^{1/2}. \quad (12)$$

274 Using $A_H \sim 10^{-18}$ J [40] and $\gamma \sim 1$ mN/m [43], we obtained $h^* \sim 10^{-8}$
 275 m, in good agreement with our experimental observations.

276 In the present study, we showed that rupture can be suppressed for $B \sim$
 277 $3A$. Assuming that our simple model can be employed in the case of a

278 multilayer system too, and putting back dimensions through Equation (2),
279 we get a critical shear rate for rupture suppression:

$$\beta_s \sim \frac{A_H}{3\pi\eta h_0^3}. \quad (13)$$

280 Using $h_0 \sim h^*$ and the values of the physical parameters provided above,
281 we obtain $\beta_s \approx 10 \text{ s}^{-1}$. Interestingly, the latter value is typical of shear rates
282 occurring during nanolayer coextrusion [44]. Since β_s decreases rapidly as h_0
283 increases, it may explain why stable layers with thicknesses as small as 20 nm
284 can be formed via this process – despite a processing time ($\sim 1 \text{ min}$) much
285 larger than the rupture times predicted by Vrij, Ruckenstein and Sharma in
286 a no-shear situation ($\sim 1 \text{ s}$, see equation 10).

287 4. Conclusion

288 We have developed a numerical model to study the effect of shear on
289 the stability of an ultra-thin polymer film, taking into account capillary and
290 vdW forces. We identified three regimes: i) a rupture regime at low shear
291 rates, with a rupture time systematically larger than the one in the no-shear
292 case, the latter being in agreement with the expressions predicted by Vrij,
293 Ruckenstein and Sharma; ii) a transient regime in which shear and Hamaker
294 forces compete with each other over the whole time window, leading to a
295 non-monotonic temporal variation of the perturbed interface; iii) a regime
296 at high shear rates in which shear suppresses rupture: a perturbed interface
297 will evolve towards a flat interface over time. Interestingly, while a linear
298 analysis is sufficient to describe the rupture time in the absence of shear,
299 the nonlinearities appear to be crucial in presence of moderate shear. This
300 study paves the way to a better analysis and control of the stabilizing and
301 destabilizing effects in nanocoextrusion processes.

302 Acknowledgements

303 The authors would like to thank the Ecole Doctorale Sciences des Métiers
304 de l'Ingénieur (ED SMI 432) for the PhD grant of K.K. and for the 3-month
305 extension during the Covid19 pandemic. The authors also acknowledge fund-
306 ing from the Agence Nationale de la Recherche (grant ANR-21-ERCC-0010-
307 01 EMetBrown) and thank the Soft Matter Collaborative Research Unit,
308 Frontier Research Center for Advanced Material and Life Science, Faculty of
309 Advanced Life Science at Hokkaido University, Sapporo, Japan.

310 **References**

- 311 [1] X. Zhang, Y. Xu, X. Zhang, H. Wu, J. Shen, R. Chen, Y. Xiong, L. J.,
312 S. Guo, Progress on the layer-by-layer assembly of multilayered polymer
313 composites: Strategy, structural control and applications, *Prog. Polym.*
314 *Sci.* 89 (2019) 76–107.
- 315 [2] L. Zhenpeng, A. Olah, E. Baer, Micro-and nano-layered processing of
316 new polymeric systems, *Prog. Polym. Sci.* 102 (2020) 101210.
- 317 [3] J. M. Carr, D. S. Langhe, M. T. Ponting, A. Hiltner, E. Baer, Confined
318 crystallization in polymer nanolayered films: A review, *J. Mater. Res.*
319 27 (2012) 1326.
- 320 [4] K. Arabeche, L. Delbreilh, R. Adhikari, G. H. Michler, A. Hiltner,
321 E. Baer, J. M. Saiter, Study of the cooperativity at the glass transition
322 temperature in PC/PMMA multilayered films: influence of thickness
323 reduction from macro-to nanoscale, *Polymer* 53 (2012) 1355–1361.
- 324 [5] R. Casalini, L. Zhu, E. Baer, C. M. Roland, Segmental dynamics and the
325 correlation length in nanoconfined PMMA, *Polymer* 88 (2016) 133–136.
- 326 [6] X. Monnier, S. F. Nassar, S. Domemek, A. Guinault, C. Sollogoub,
327 E. Dargent, N. Delpouve, Reduced physical aging rates of polylactide in
328 polystyrene/polylactide multilayer films from fast scanning calorimetry,
329 *Polymer* 150 (2018) 1–9.
- 330 [7] R. Y. F. Liu, T. E. Bernal-Lara, A. Hiltner, E. Baer, Polymer interphase
331 materials by forced assembly, *Macromolecules* 38 (2005) 4819–4827.
- 332 [8] R. Y. F. Liu, A. P. Ranade, H. P. Wang, T. E. Bernal-Lara, A. Hiltner,
333 E. Baer, Forced assembly of polymer nanolayers thinner than the
334 interphase, *Macromolecules* 38 (2005) 10721–10727.
- 335 [9] Q. Beuguel, A. Guinault, L. Leger, F. Restagno, C. Sollogoub,
336 G. Miquelard-Garnier, Nanorheology with a conventional rheometer:
337 Probing the interfacial properties in compatibilized multinanopolymer
338 films, *ACS Macro Letters* 8 (2019) 1309–1315.
- 339 [10] M. Ponting, A. Hiltner, E. Baer, Polymer Nanostructures by Forced As-
340 sembly: Process, Structure and Properties, *Macromolecular Symposia*
341 (2010) 19–32.

- 342 [11] S. Scholtyssek, R. Adhikari, V. Seydewitz, G. H. Michler, E. Baer,
343 A. Hiltner, Evaluation of morphology and deformation micromech-
344 anisms in multilayered PP/PS films: an electron microscopy study,
345 *Macromolecular Symposia* 294 (2010) 33–44.
- 346 [12] K. Ho, J. S. Lee, N. Viriyabanthorn, C. S. C. M. F. Barry, J. L. Mead,
347 Interfacial instabilities in multilayer extrusion, in: M. Laudon, B. Ro-
348 manowicz (Eds.), *Nanotechnology Conference and Trade Show (Nan-*
349 *otech)*, volume 3, Boston, MA, 2004, pp. 468–471.
- 350 [13] J. Feng, Z. Zhang, A. Bironeau, A. Guinault, G. Miquelard-Garnier,
351 C. Sollogoub, A. Olah, E. Baer, Breakup behavior of nanolayers in
352 polymeric multilayer systems—creation of nanosheets and nanodroplets,
353 *Polymer* 143 (2018) 19–27.
- 354 [14] A. Bironeau, T. Salez, G. Miquelard-Garnier, C. Sollogoub, Existence
355 of a Critical Layer Thickness in PS/PMMA Nanolayered Films, *Macro-*
356 *molecules* 50 (2017) 4064–4073.
- 357 [15] G. Reiter, Dewetting of thin polymer films, *Phys. Rev. Lett.* 68 (1992)
358 75–78.
- 359 [16] F. Brochard-Wyart, P. Martin, C. Redon, Liquid/Liquid Dewetting,
360 *Langmuir* 9 (1993) 3682–3690.
- 361 [17] Y. Zhu, A. Bironeau, F. Restagno, C. Sollogoub, G. Miquelard-Garnier,
362 Kinetics of thin polymer film rupture: Model experiments for a better
363 understanding of layer breakups in the multilayer coextrusion process,
364 *Polymer* 90 (2016) 156–164.
- 365 [18] M. S. Chebil, J. D. McGraw, T. Salez, C. Sollogoub, G. Miquelard-
366 Garnier, Influence of outer-layer finite-size effects on the rupture kinetics
367 of a thin polymer film embedded in an immiscible matrix, *Soft Matter*
368 14 (2018).
- 369 [19] C. A. Powell, M. D. Savage, J. T. Guthrie, Modelling printing pro-
370 cesses: A computational approach, *Surface Coatings International Part*
371 *B: Coatings Transactions* 88 (2005) 171–176.
- 372 [20] R. D. Lenz, S. Kumar, Instability of confined thin liquid film trilayers,
373 *J. Colloid Int. Sci.* 316 (2007) 660–670.

- 374 [21] A. Oron, S. H. Davis, S. G. Bankoff, Long-scale evolution of thin liquid
375 films, *Rev. Mod. Phys.* 69 (1997) 931–980.
- 376 [22] R. V. Craster, O. K. Matar, Dynamics and stability of thin liquid films,
377 *Rev. Mod. Phys.* 81 (2009) 1131–1198.
- 378 [23] A. Vrij, Possible Mechanism for the Spontaneous rupture of thin Free
379 Liquid Films, *Discussions Faraday Society* 42 (1966) 23–33.
- 380 [24] A. Sheludko, Thin liquid films, *Adv. Colloid Interface Sci.* 1 (1967)
381 391–464.
- 382 [25] E. Ruckenstein, R. Jain, Spontaneous rupture of thin liquid films, *J.*
383 *Chem. Soc., Faraday Trans.* 70 (1974) 132–147.
- 384 [26] B. V. Derjaguin, The definition and magnitude of disjoining pressure
385 and its role in the statics and dynamics of thin fluid films, *Kolloid Zh.*
386 (1955) 207–214.
- 387 [27] A. Sharma, E. Ruckenstein, An analytical nonlinear theory of thin film
388 rupture and its application to wetting films, *J. Colloid Int. Sci.* 113
389 (1986) 456–479.
- 390 [28] M. B. Williams, S. H. Davis, Nonlinear theory of film rupture, *J. Colloid*
391 *Int. Sci.* 90 (1982) 220–228.
- 392 [29] D. Bandyopadhyay, R. Gulabani, A. Sharma, Instability and Dynamics
393 of Thin Liquid Bilayers, *Ind. Eng. Chem. Res.* (2005) 1259–1272.
- 394 [30] A. Pototsky, M. Bestehorn, D. Merkt, U. Thiele, Alternative pathways
395 of dewetting for a thin liquid two-layer film, *Phys. Rev. E* 70 (2004) 4.
- 396 [31] S. K. Kalpathy, L. F. Francis, S. Kumar, Shear-induced suppression of
397 rupture in two-layer thin liquid films, *J. Colloid Int. Sci.* 348 (2010)
398 271–279.
- 399 [32] M. J. Davis, M. B. Gratton, S. H. Davis, Suppressing van der Waals
400 driven rupture through shear, *J. Fluid Mech.* 661 (2010) 522–529.
- 401 [33] M. Thiébaud, T. Bickel, Nonequilibrium fluctuations of an interface
402 under shear, *Phys. Rev. E* 81 (2010) 1–13.

- 403 [34] M. Thiébaud, Y. Amarouchene, T. Bickel, Nonlinear Brownian dynam-
404 ics of interfacial fluctuations in a shear flow, *J. Stat. Mech.* 2014 (2014).
- 405 [35] T. Salez, J. D. McGraw, S. L. Cormier, O. Bäumchen, K. Dalnoki-
406 Veress, E. Raphaël, Numerical solutions of thin-film equations for poly-
407 mer flows, *Eur. Phys. J. E* 35 (2012) 1–9.
- 408 [36] A. L. Bertozzi, *The Mathematics of Moving Contact Lines in Thin*
409 *Liquid Films*, *Notices of the AMS* 45 (1998) 676–680.
- 410 [37] L. Zhornitskaya, A. L. Bertozzi, Positivity-preserving numerical schemes
411 for lubrication-type equations, *SIAM J. Numer. Anal.* 37 (2000) 523–
412 555.
- 413 [38] S. Wu, Surface and interfacial tensions of polymer melts: Ii. poly(methyl
414 methacrylate), poly(n-butyl methacrylate), and polystyrene, *J. Phys.*
415 *Chem.* 74 (1970) 632–638.
- 416 [39] R. Seemann, S. Herminghaus, K. Jacobs, Dewetting patterns and molec-
417 ular forces: A reconciliation, *Phys. Rev. Lett.* 86 (2001) 5534–5537.
- 418 [40] J. P. de Silva, F. Cousin, A. R. Wildes, M. Geoghegan, M. Sferrazza,
419 Symmetric and asymmetric instability of buried polymer interfaces,
420 *Phys. Rev. E* 86 (2012) 032801.
- 421 [41] J. N. Israelachvili, *Intermolecular and Surface Forces*, Academic Press,
422 London, 1991.
- 423 [42] T. Sarlat, A. Lelarge, E. Søndergård, D. Vandembroucq, Frozen capil-
424 lary waves on glass surfaces: An AFM study, *Eur. Phys. J. B* 54 (2006)
425 121–126.
- 426 [43] G. Miquelard-Garnier, S. Roland, Beware of the flory parameter to
427 characterize polymer-polymer interactions: A critical reexamination of
428 the experimental literature, *Eur. Polym. J.* 84 (2016) 111–124.
- 429 [44] A. Bironeau, *Films multianocouches de polymères amorphes coex-*
430 *trudés : Élaboration, caractérisation et stabilité des nanocouches*, Ph.D.
431 thesis, ENSAM, 2017.